Clays and Clay Minerals, Vol. 54, No. 5, 616–625, 2006.

FUZZY PHASE DIAGRAMS OF CLAY MINERALS

CHANDRIKA VARADACHARI*
Raman Centre for Applied and Interdisciplinary Sciences, 16A Jheel Road, Calcutta 700 075, India

Abstract—This paper presents a novel concept in the thermodynamic derivation of phase diagrams for clay minerals that incorporates fuzzy transition zones. This new technique yields phase diagrams that have graded (fuzzy) zones of mineral occurrences and includes compositional variability within mineral groups. For the construction of these diagrams, 170 minerals belonging to nine different subgroups were used, based on a fuzzy mathematical description of their 'grades' or 'belonging-ness'. Standard free energies of formation of all the minerals were derived and all possible pairs of mineral equilibria were evaluated. Relative intensities of mineral occurrences were determined and membership values of each type of mineral at various zones in a 2D or 3D space were graphically represented. Computations and graphical representations were carried out using programs developed in *Mathematica*. Diagrams were derived for 25ºC, 1 bar with a solution phase containing $Si(OH)_4$, K^+, Na^+, H^+, Ca^{2+} and Mg^{2+} under conditions of gibbsite, goethite and ferrous oxide saturation. The resulting diagrams, unlike conventional phase diagrams, show multimineral assemblages, with varying occurrences of different minerals and provide a realistic representation of clay mineral occurrences formed by surface geochemical processes. They show that on the Earth's surface, only montmorillonite can almost completely predominate the inorganic phase followed by kaolinite, illite and beidellite. Nontronite, glauconite, celadonite and vermiculite would not be neoformed in substantial amounts. A general conformity of derived phase equilibria with experimentally observed equilibria is also observed.

Key Words—Equilibria, Free Energy, Fuzzy, Illite, Kaolinite, Montmorillonite, Phase, Program, 2D, 3D.

INTRODUCTION

The presence of clay minerals on Earth as well as on extraterrestrial materials such as meteorites is indicative of a hydrogeological environment and can be useful in tracing their environmental history of formation. The utility of phase diagrams as a tool for understanding the geochemical history of clay minerals is limited by the fact that existing thermodynamic methods (Garrels and Christ, 1965; Helgeson *et al*., 1969; Varadachari, 1992; Tardy and Duplay, 1994) result in mineral phase diagrams showing only single phases with sharply defined boundaries whereas nature abounds with multimineral assemblages with gradual transitions from one phase to another. The complexity and diffuseness of clay mineral compositions and the rarity of their occurrence in the pure state makes it difficult to find theoretical models to provide a realistic picture. Existing methods are based on traditional mathematical concepts that assume crisp and precise situations and cannot accommodate the vagueness inherent in clay mineral compositions and occurrences.

Fuzzy set theory (Klir and Yuan, 1997) provides a mathematical framework that is more appropriate for handling the complexity of such systems. The utility of fuzzy mathematics in analyzing and understanding the compositional heterogeneity of clay minerals was shown by Varadachari *et al.* (2003). Using the framework of fuzzy mathematics, they derived a methodology to quantify (1) the grade or 'belonging-ness' of a clay mineral to its own group or subgroup and (2) the 'resemblance' or compositional overlap to other groups or subgroups.

Here, an attempt was made to incorporate the concepts of fuzzy logic in the thermodynamic derivation of phase diagrams of clay minerals. Derivations included numerous clays of varying chemical compositions and grades. The resulting fuzzy phase diagrams provide a more realistic model of mineral equilibria that can accommodate a range of compositional variability, can represent mineral admixtures, and have gradual transition zones replacing sharp phase boundaries. We thus have for the first time a model of multimineral assemblages under various surface geochemical conditions.

METHODOLOGY

A data set of 464 clay minerals available as on-line material (Varadachari *et al.*, 2003) was the starting point from which the present data set was derived. The dataset contains compositional and other data on smectites (montmorillonites, beidellites, nontronites and saponites), clay micas (illites, glauconites and celadonites) and vermiculites. To maintain charge neutrality in the chemical formula, minor adjustments of exchangeable

* E-mail address of corresponding author:
RCAIS@CAL3.VSNL.NET.IN
DOI: 10.1346/CCMN.2006.0540508

cation levels were sometimes necessary. Thus, an excess negative charge of 0.002 was balanced by increasing exchangeable Ca^{2+} by 0.001. Composition data that showed large imbalances in charge neutrality were rejected. The data were then statistically analyzed by linear discriminant analysis (Varadachari and Mukherjee, 2004), which showed that the minerals are compositionally distinct and can be statistically classified into eight subgroups. Thus, despite the possibility that some incorrect composition data are included in the data set, the collective error is statistically low and compositional differences among clay mineral subgroups can be clearly distinguished.

From the derived grades (fuzzy membership values) (Varadachari *et al.*, 2003) a selection was made of minerals which have a grade $\geqslant 0.5$ at the group as well as subgroup levels. This is a cut-off to ensure that only minerals that are fairly representative are included and those with compositional or classification errors are excluded. For example, only illites with grades of 0.5 or more in the clay mica group and also in the illite subgroup were selected. Thereby minerals that are compositionally very poorly illitic or compositionally extreme or are misclassified are all excluded from the derivations. Thus, we have a data set for 170 minerals (Table S1 in supporting online material: www.clays.org/journal/JournalDeposits.html) that provides chemical composition data, literature sources, group and subgroup membership values and standard free energies of formation (ΔG_f^0). In the absence of experimental thermodynamic data for most of the minerals, ΔG_f^0 data were derived by a regression method that utilizes an iterative least-squares fitting to solve an exponential non-linear equation to obtain ΔG_f^0 (Varadachari *et al.*, 1994; Kudrat *et al.*, 1999, 2000). Estimates of ΔG_f^0 obtained by this method showed good agreement with standard experimental data for end-member minerals as well as non-stoichiometric clays such as illites, montmorillonites and chlorites (Varadachari *et al.*, 1994; Kudrat *et al.*, 2000). Primary thermodynamic data used for these derivations were taken from the collection by Johnson *et al.* (1992).

Utilizing the derived values of ΔG_f^0, computations of the standard free energy change for crystallization (ΔG_c^0) from solution were performed (Varadachari, 1992; Varadachari and Ghosh, 2003). For example, the ΔG_c^0 for a montmorillonite of composition $K_{0.4}Si_{3.83}Al_{1.67}Mg_{0.38}Fe(III)_{O.17}O_{10}(OH)_2$ was evaluated as the free energy change of the reaction

$$0.38Mg^{2+} + 0.4K^+ + 0.17FeO(OH) + 1.67Al(OH)_3 + 3.83Si(OH)_4 \rightleftharpoons K_{0.4}Si_{3.83}Al_{1.67}Mg_{0.38}Fe(III)_{0.17}O_{10}(OH)_2 + 1.16H^+ + 8.67H_2O \quad (1)$$

Thermodynamic data for cations and water were taken from the literature (Robie *et al.*, 1978; Johnson *et al.*, 1992). This reaction represents equilibrium between a mineral and its components and can be viewed as a crystallization reaction in the forward direction and a dissolution reaction in the reverse direction.

Primary components for the calculated phase diagrams were $Si(OH)_4$, K^+, Mg^{2+}, Ca^{2+}, Na^+, H^+, H_2O, $Al(OH)_3$, FeO(OH) and FeO. Here the components were selected to (1) model an environment that is not too highly acidic or alkaline so that the end-product of weathering is gibbsite and (2) contain both ferrous and ferric compounds as many clay minerals contain both Fe^{3+} and Fe^{2+} in their structure. Under these conditions, because of the low solubility of Al^{3+} and $Fe^{3+/2+}$, only their solid phases (gibbsite and goethite, respectively) would be stable. Activities of Al^{3+} and Fe^{3+} in solution would thus be controlled by the dissolution of gibbsite and goethite so that the reaction occurs in stages that pass through a solution phase of Al and Fe such as

$$0.17FeO(OH) + 1.67Al(OH)_3 + 5.52H^+ \rightleftharpoons 0.17Fe^{3+} + 1.67Al^{3+} + 5.35H_2O \quad (2)$$

$$0.38Mg^{2+} + 0.4K^+ + 0.17Fe^{3+} + 1.67Al^{3+} + 3.83Si(OH)_4 \rightleftharpoons K_{0.4}Si_{3.83}Al_{1.67}Mg_{0.38}Fe(III)_{0.17}O_{10}(OH)_2 + 6.68H^+ + 3.32H_2O \quad (3)$$

By combining reactions 2 and 3, we have

$$[0.17FeO(OH) + 1.67Al(OH)_3 + 5.52H^+] + [0.38Mg^{2+} + 0.4K^+ + 0.17Fe^{3+} + 1.67Al^{3+} + 3.83Si(OH)_4] \rightleftharpoons [0.17Fe^{3+} + 1.67Al^{3+} + 5.35H_2O] + [K_{0.4}Si_{3.83}Al_{1.67}Mg_{0.38}Fe(III)_{0.17}O_{10}(OH)_2 + 6.68H^+ + 3.32H_2O] \quad (4)$$

Simplifying equation 4, it reduces to

$$0.38Mg^{2+} + 0.4K^+ + 0.17FeO(OH) + 1.67Al(OH)_3 + 3.83Si(OH)_4 \rightleftharpoons K_{0.4}Si_{3.83}Al_{1.67}Mg_{0.38}Fe(III)_{0.17}O_{10}(OH)_2 + 1.16H^+ + 8.67H_2O$$

which is the same as equation 1 above. This signifies that although the reaction may occur in several stages involving dissolution of gibbsite, formation of various types of soluble Al species *etc*., for thermodynamic purposes, we consider only the initial and final stages, and the reaction may be represented as in equation 1. Effectively, therefore, the activities of soluble Al and Fe species need not be considered and the activities of all solids, in accordance with thermodynamic conventions, are taken as unity ($a = 1$).

The diagrams can, if necessary, be constructed with Al and Fe in the solution phase (as Al^{3+}, $Al(OH)^{2+}$, $Fe^{3+/2+}$, *etc*.). This would reflect conditions of high acidity when gibbsite or goethite would no longer remain in the solid phase and would not control Al or Fe activities. The choice of components used here is intended to represent a more generalized environment of clay mineral neoformation under surface conditions.

Clay minerals that can be constituted from these components include 170 minerals belonging to nine

mineral subgroups, *i.e.* illites, glauconites, celadonites, montmorillonites, beidellites, nontronites, saponites and kaolinites (Table S1, listing the clay mineral compositions, membership values and thermodynamic values is available from The Clay Mineral Society's website – journal deposits page: http://www.clays.org/journal/JournalDeposits.html).

The free energy change of crystallization (ΔG_c) is related to the activities in solution of $Si(OH)_4$, K^+, Na^+, Ca^{2+} and Mg^{2+}. The influence of solution activity on ΔG_c for each mineral, therefore, varies and may be expressed as

$$\Delta G_c = \Delta G_c^0 + RT\ln\,[a_H^{\eta}/a_{Si}^{\sigma}.a_K^{\kappa}.a_{Mg}^{\lambda}.a_{Ca}^{\chi}.a_{Na}^{\nu}] \quad (5)$$

where a_{Si}, a_K, a_{Mg}, a_{Ca}, a_{Na} and a_H refer to the activities of the $Si(OH)_4$, K^+, Mg^{2+}, Ca^{2+}, Na^+ and H^+ in solution, the power terms refer to the formula fractions of these cations in the mineral and $\eta = \kappa + 2\lambda + 2\chi + \nu$. The ΔG_c of each mineral was evaluated over a range of activities and was compared with the ΔG_c of every mineral of every other group. Between each of these pairs of equilibria, the mineral having the more negative value of ΔG_c is the (meta)stable phase. Thus, all possible pairs of mineral equilibria were computed.

For computing zonal grades or membership functions, μ_z (Klir and Yuan, 1997), each metastable phase was given equal weight. The density of occurrence of a mineral relative to the total was then computed on a scale of 0 to 1. For example, if we have p samples of different compositions belonging to mineral type A and q samples of different compositions belonging to mineral type B, the computed ΔG_c values are α_1, α_2, ... α_p and β_1, β_2, ... β_q at a defined value of the solution activities $a_{Si} = x$, $a_K = y$, $a_{Mg} = k$, $a_{Ca} = m$ and $a_{Na} = n$, *i.e.* a single point on an x-y plane with the other three variables as constants. Then α_1 is compared with β_1, β_2 ..... β_q. If $\alpha_1 < \beta_1$, then α_1 is assigned to the point x-y and given a weight of 1; otherwise if $\alpha_1 > \beta_1$, then β_1 is assigned to the point x-y

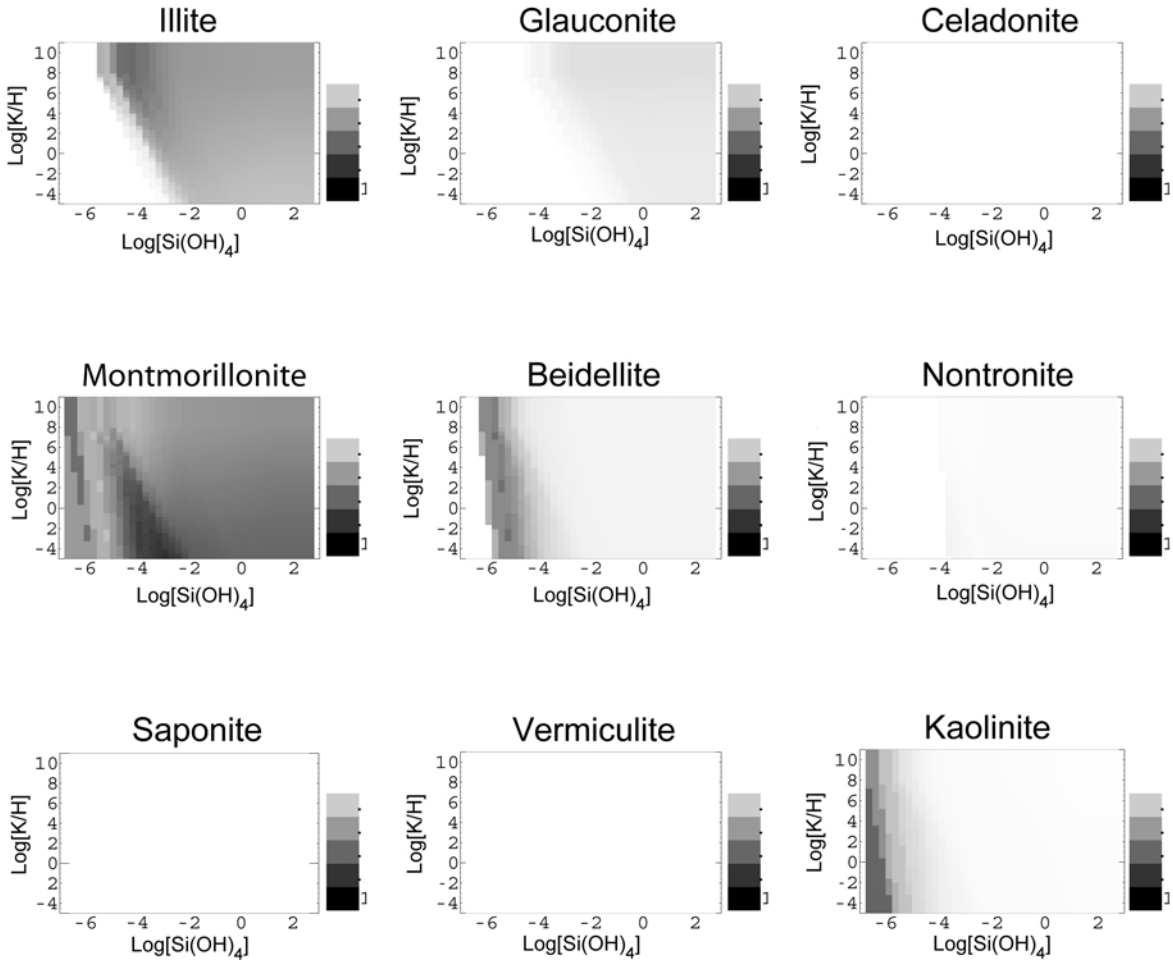

Figure 1. (a) Fuzzy phase diagrams showing graded zones of mineral occurrences in a $\log[Si(OH)_4] - \log[K^+/H^+]$ space (at $\log[Mg^{2+}/(H^+)^2] = -2$, $\log[Na^+/H^+] = -4$, $\log[Ca^{2+}/(H^+)^2] = -2$). The diagram is constructed for 25ºC and 1 bar in an aqueous environment containing gibbsite, goethite and ferrous oxide. The solid components and water have activity of 1. The relative intensity of each mineral phase is indicated by the intensity of the color and can be assessed using values given in the label box.

and given a weight of 1. The process is repeated so that all possible α-β comparisons are made. The weight of α and β values are computed and described as a fraction, μ_z, of the total. This number, on a scale of 0 to 1 describes the intensity of occurrence of the minerals *A* and *B* at one point, *x-y*, on a 2D graphical representation. Where several types of minerals (*A*, *B*, *C*, ⋯*N*) are considered, the same procedure is extended to include the comparisons *A*−*B*, *A*−*C*, ⋯*A*−*N*, *B*−*C*, ⋯, *B*−*N*, *etc*. Thereby ΔG_c values of all minerals in all mineral groups *A* to *N* are compared. The process is repeated over the entire range of *x*−*y* (for a 2D representation) or *x-y-z* (for a 3D representation). The resulting data represent the zonal grades of mineral occurrences.

Here, computations were performed at periodic intervals of 0.25 of the variable a_{Si} and 0.4 of the variables a_K or a_{Mg}, after assigning constant values to the other variables, a_{Na}, a_{Ca} and a_{Mg} or a_K. Programs were developed in *Mathematica* and 2D or 3D representations of graded mineral zones were obtained. (These programs are accessible from The Clay Mineral Society's website: www.clays.org/journal/JournalDeposits.html).

In constructing the diagrams, the activities of all solid components (gibbsite, goethite and clay minerals) are

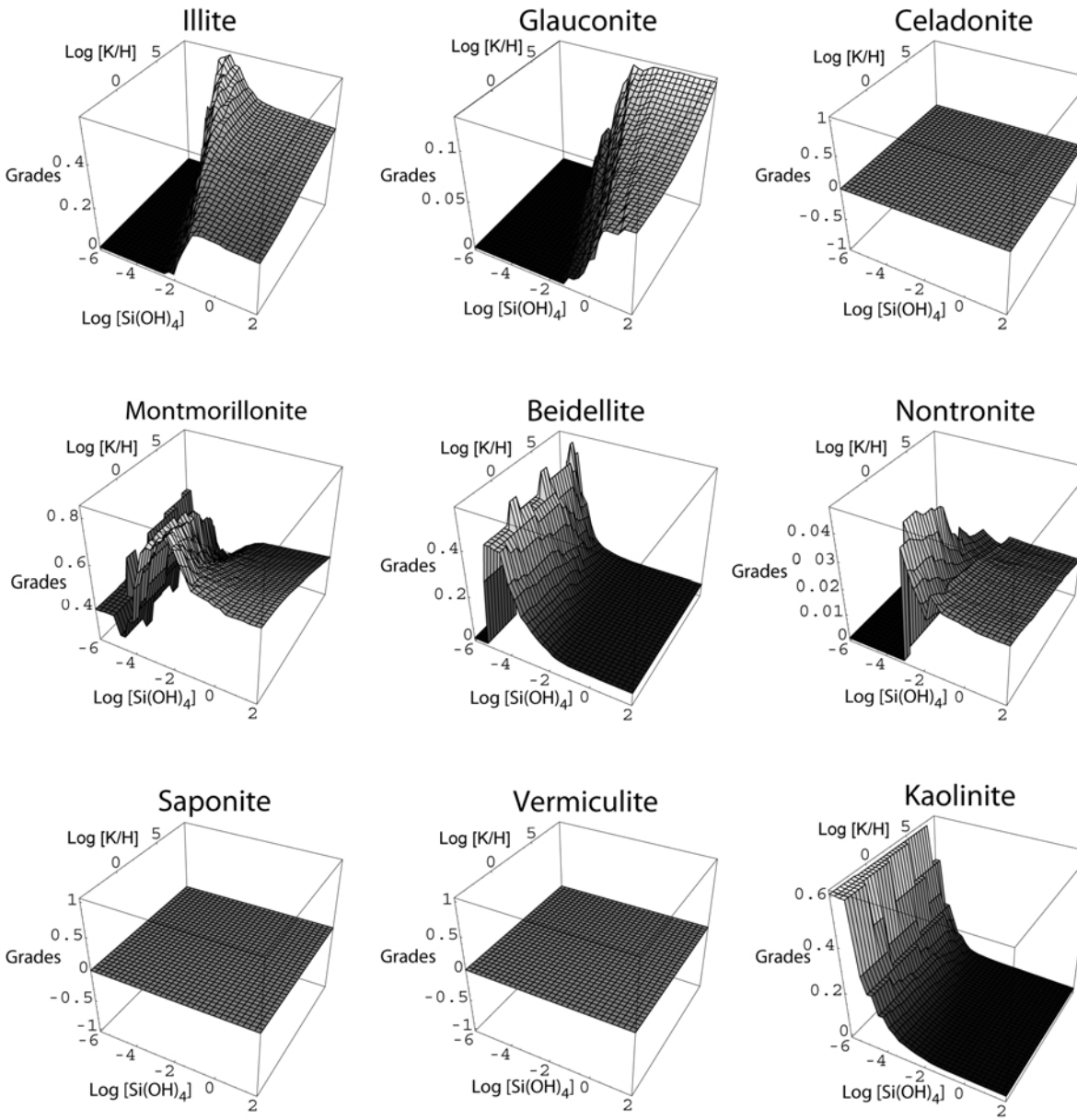

Figure 1. (b) 3D representation showing zonal grades (intensities of occurrences) along the *z* axis. Note that zonal grade values are different in each graph.

taken as equal to 1. The activities of all soluble species not represented graphically have to be assigned constant values (constants in equation 5) to comply with the Phase Rule. Here, three different ranges of these constants have been chosen to represent very low to very high activities of Mg^{2+}, Na^{+} and Ca^{2+}. Diagrams have been constructed at $\log[Mg^{2+}/(H^{+})^2] = -2, 7, 16$, $\log[Na^{+}/H^{+}] = -4, 3, 8$, $\log[Ca^{2+}/(H^{+})^2] = -2, 7, 16$. These are chosen to demonstrate changes in the phases over a broad range of pH and cation levels. However, the method can be used to derive phase diagrams for any other chosen values that are assigned to the constants.

RESULTS

Figure 1a is a 2D fuzzy phase diagram of clay minerals at a temperature of 25ºC and pressure of 1 bar, plotted as a function of the logarithm of the activity of $Si(OH)_4$ and the ratio of the activities of K^{+} and H^{+}. The representation requires that the values of three other variables, *i.e.* the activities of Mg^{2+}, Na^{+} and Ca^{2+} are specified as constants and the activities of all solid phases gibbsite, goethite, ferrous oxide and clay minerals are unity. In Figure 1, the values of these constants have been fixed at $\log[Mg^{2+}/(H^{+})^2] = -2$, $\log[Na^{+}/H^{+}] = -4$ and $\log[Ca^{2+}/(H^{+})^2] = -2$; these conditions represent low pH and low activities of Mg^{2+}, Na^{+} and Ca^{2+}. The diagram shows the intensity of mineral occurrences as graded zones. Here, kaolinite is the dominant phase at $\log[Si(OH)_4] < -5$ and montmorillonite is the dominant species at $\log[Si(OH)_4] > -4$; illites and beidellites are the associated phases. Alternatively, relative distributions of the minerals may also be represented in a triaxial graph (Figure 1b) which shows the intensities of occurrences along the *z* axis. In such diagrams, the highest zonal grades can be read directly from the graph.

Another diagram showing mineral distributions in environments richer in Ca^{2+}, Mg^{2+} and Na^{+} is shown in Figure 2a. The 3D representation of this is given in Figure 2b. Under these conditions, montmorillonite can dominate with a zonal grade of ~0.8 at $\log[Si(OH)_4] \sim -3$ but kaolinite grades weaken sharply to ~0.3. Next in dominance is illite (at $\log[Si(OH)_4] > -3$) which shows a highest zonal grade of ~0.4. With further increase in Ca^{2+}, Mg^{2+}, Na^{+} and pH, *i.e.* at $\log[Mg^{2+}/(H^{+})^2] = 16$, $\log[Na^{+}/H^{+}] = 8$ and $\log[Ca^{2+}/(H^{+})^2] = 16$ (Figure 3), montmorillonite is predominant and is associated with traces of beidellite, saponite and kaolinite ($\log[Si(OH)_4] < -3$). At $\log[Si(OH)_4] > -3$, illite-montmorillonite associations are the major minerals.

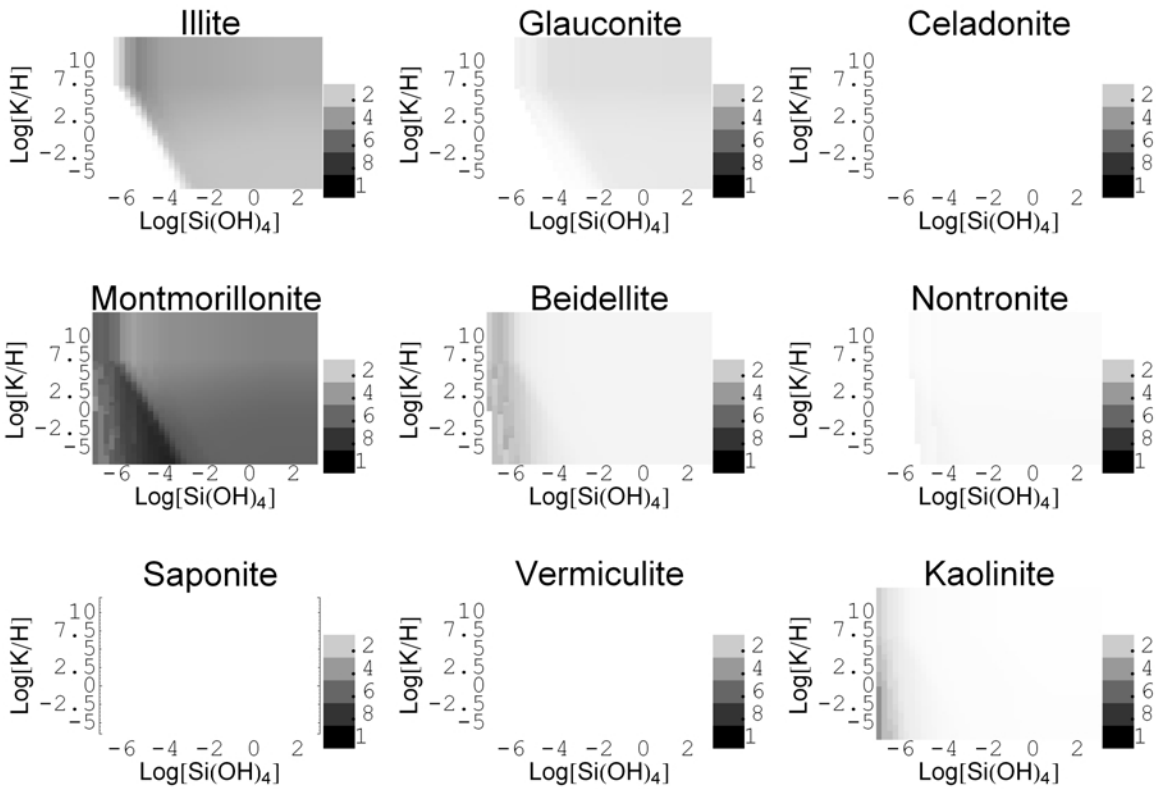

Figure 2. (a) Fuzzy phase diagrams showing graded zones of mineral occurrences in a $\log[K^{+}/H^{+}]$–$\log[Si(OH)_4]$ space (at $\log[Mg^{2+}/(H^{+})^2] = 7$, $\log[Na^{+}/H^{+}] = 3$, $\log[Ca^{2+}/(H^{+})^2] = 7$). The diagram is constructed for 25ºC and 1 bar in an aqueous environment containing gibbsite, goethite and ferrous oxide. The solid components and water have activity of 1.

An interesting observation from the diagrams is that regions of illite occurrences always contain montmorillonites as associated phases. However, the converse is not true; highly montmorillonitic formations can occur where illites are negligible.

The phase diagrams can also be represented on a 3-dimensional axis showing $\log[Si(OH)_4]-\log[K^+/H^+]-\log[Mg^{2+}/(H^+)^2]$ as variables. The resulting figure (at $\log[Na^+/H^+] = 3$ and $\log[Ca^{2+}/(H^+)^2] = 7$) shows the highest possible zonal grades for various minerals and the conditions under which they may occur (Figure 4). Highest zonal grades are observed with montmorillonite (~0.8) followed by kaolinite (~0.6), illite and beidellite (~0.5). Occurrences of other minerals such as glauconite, nontronite, celadonite and vermiculite are very weak and their presence in substantial amounts on surfaces or sediments would, therefore, suggest genesis routes other than neoformation.

It may be inferred from the diagrams that surface neoformation processes would generally yield clay mineral admixtures; nearly pure phases would be rare and suggest extreme environments. Amongst the various types of clay minerals, only montmorillonite can almost completely dominate the inorganic phase in soils. Illites and beidellites would occur in association with montmorillonite and would never dominate the soil mineral phase. Kaolinite is the only other clay mineral that could constitute a major part of the soil mineral phase. This provides an explanation for the interesting phenomena that although black soils (Vertisols), can be highly montmorillonitic, there are no other soils whose mineral matrix is equally dominant with respect to other clay minerals like illite, glauconite, vermiculite, *etc.*

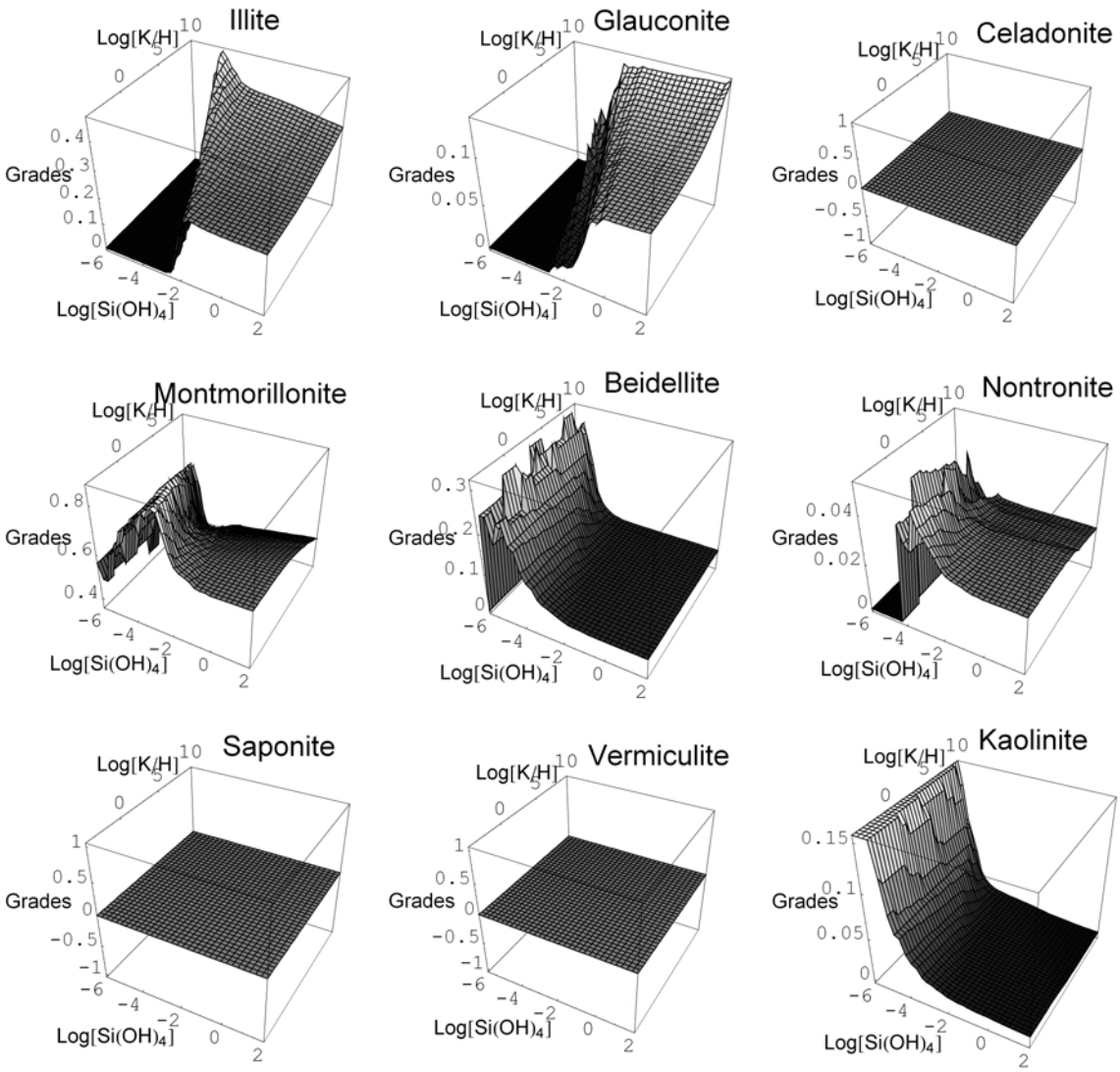

Figure 2. (b) 3D representation of Figure 2a showing zonal grades (intensities of occurrences) along the *z* axis. Note that zonal grade values are different in each graph.

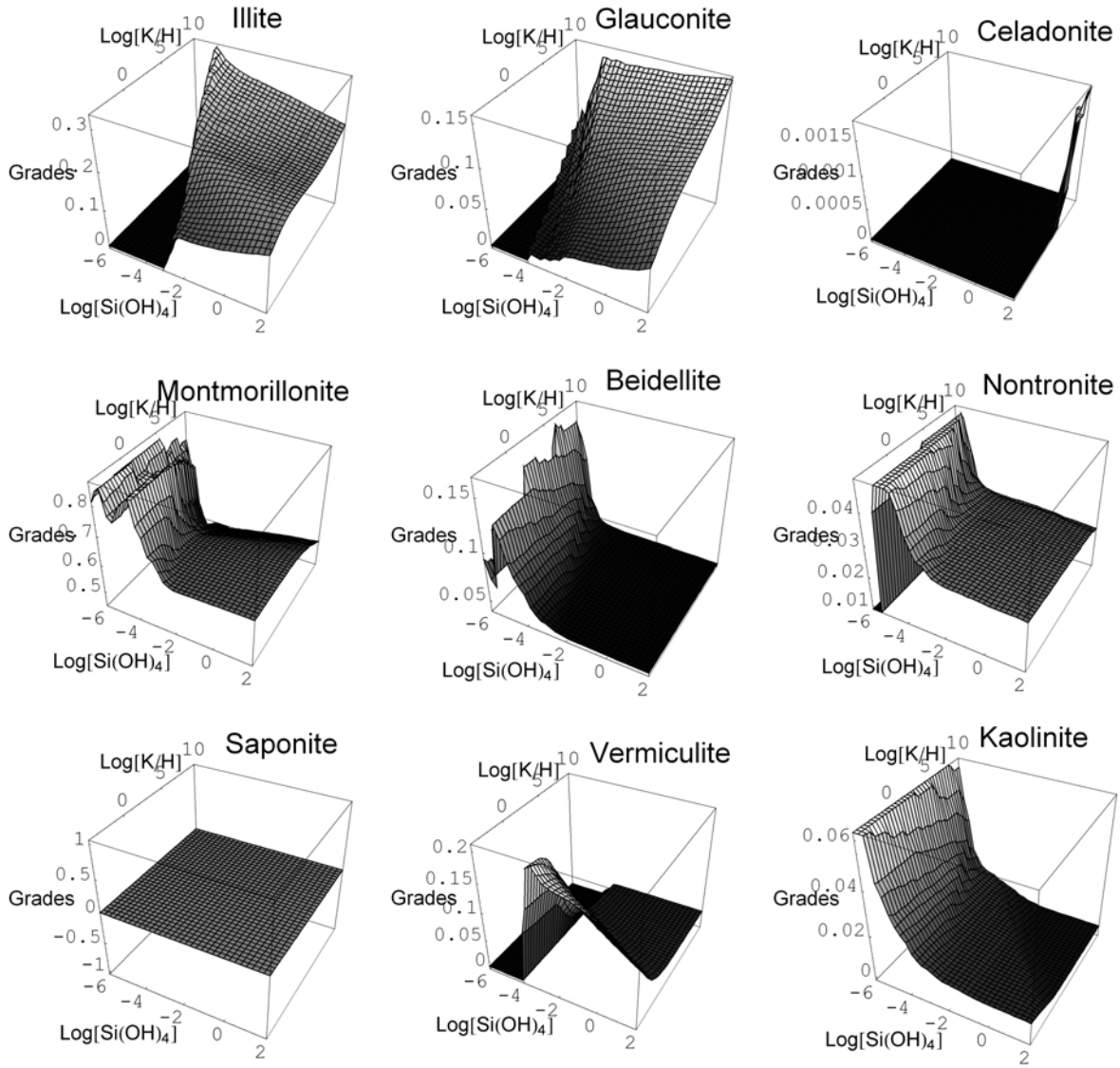

Figure 3. 3D fuzzy phase diagrams in a $\log[K^+/H^+]$– $\log[Si(OH)_4]$ space (at $\log [Mg^{2+}/(H^+)^2] = 16$, $\log [Na^+/H^+] = 8$, $\log [Ca^{2+}/(H^+)^2] = 16$). The diagram is constructed for 25ºC and 1 bar in an aqueous environment containing gibbsite, goethite and ferrous oxide. Solid components and water have activity of 1. Note that zonal grade values are different in each graph.

Comparisons of mineral occurrences as predicted by the phase diagrams were attempted with water chemistry of natural and experimental systems. The compositions of stream waters analyzed by Norton (1974) are predicted from these derivations to have a predominantly montmorillonitc mineralogy (of grade ~0.7) with associated kaolinite (of grade ~0.1); this agrees with the observed clay mineralogy of the region which is montmorillonite with associated kaolinite and gibbsite. Water analysis of springs and wells in largely montmorillonitic regions of Chad, Senegal and also Brittany (Tardy, 1971) correlate with predicted montmorillonite occurrences of 0.6–0.8. Similarly, good correlations are also observed in chemical compositions of Lake Chad (samples C and D) which have montmorillonite-beidellite associations (Tardy and Duplay, 1994); here, in addition to montmorillonite and beidellite (grade ~0.6), the presence of illite (grade ~0.3) is also predicted. Experimental data on illite equilibria (at 25ºC in the presence of gibbsite-kaolinite) provide solution compositions (Aja *et al.*,1991) that correspond to a calculated zone of illite dominance (grade ~0.5) together with montmorillonite (grade ~0.35). Aja *et al*. (1991) observed that the compositions of these equilibrating phases are illite and smectite.

CONCLUSIONS

A methodology has been derived for the construction of fuzzy phase diagrams of clay minerals. This new

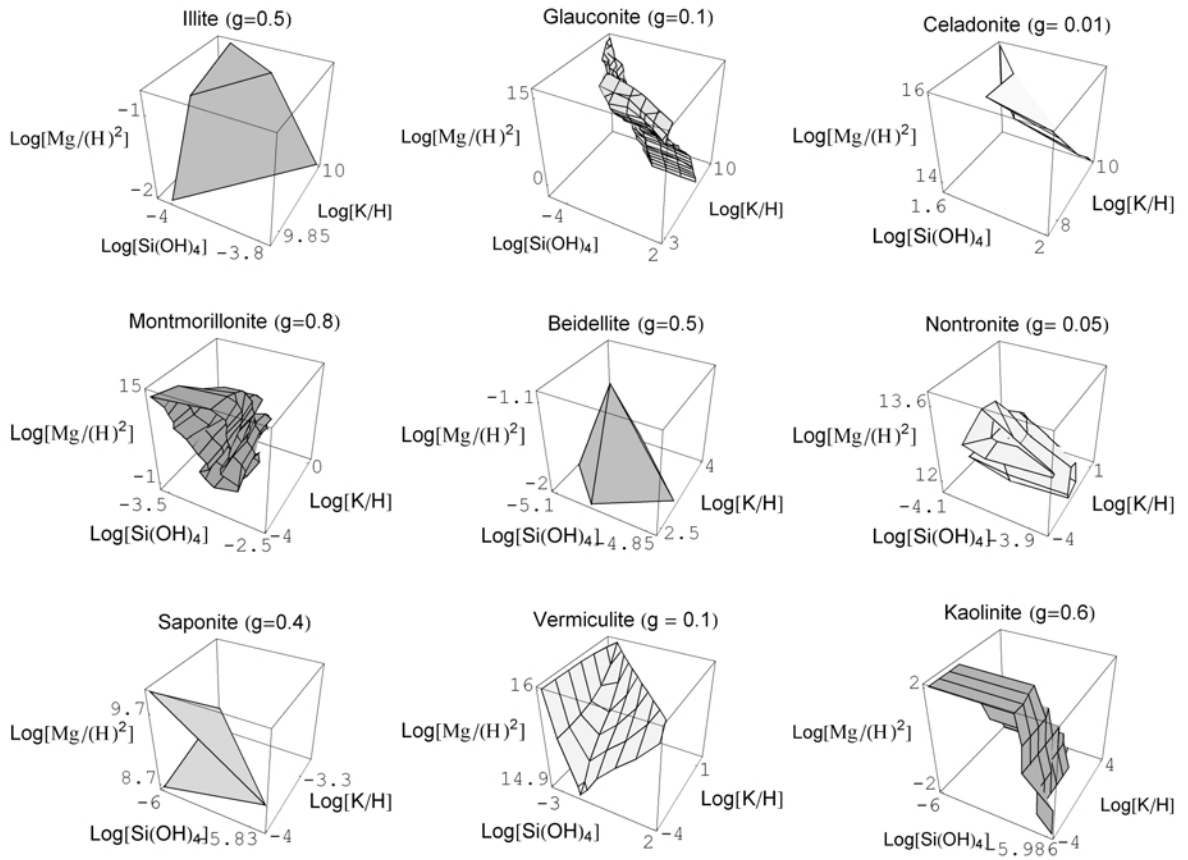

Figure 4. Triaxial diagram in a $\log[K^+/H^+] - \log[Si(OH)_4] - \log [Mg^{2+}/(H^+)^2]$ space (at $\log [Na^+/H^+] = 3$, $\log [Ca^{2+}/(H^+)^2] = 7$) showing contour regions of highest zonal grades for each clay mineral. The diagram is constructed for 25ºC and 1 bar in an aqueous environment containing gibbsite, goethite and ferrous oxide. Solid components and water have activity of 1.

approach provides a process for deriving phase diagrams of clay mineral assemblages and the intensities of their occurrences. The procedure is illustrated for a system containing variables $Si(OH)_4$, K^+, Na^+, Ca^{2+}, Mg^{2+} and H^+, under conditions of gibbsite, goethite and ferrous oxide saturation at standard temperature and pressure. However, the conditions used here are only illustrative and not restrictive and the procedure can be readily adapted to other variables and different datasets having any number of clay minerals.

The methodology also provides a theoretical model for natural observations of clay mineral associations in soils and the relative dominance of a few. Amongst the smectites, occurrences of montmorillonite are predicted to be dominant compared to saponite, nontronite or beidellite, in environments of neoformation, such as in soils; similarly, illite occurrences would prevail amongst the clay micas. Thermodynamic derivations also suggest that of all clay minerals, montmorillonite is the species that would occur in greatest abundance in surface neoformed environments and illite would usually be associated with montmorillonite. The consistently low grades for occurrences of minerals like celadonite, glauconite, saponite, *etc*. suggest that fuzzy phase diagrams could probably also be used as a tool for delineating neoformed clay minerals from inherited minerals, and thereby tracing the genesis of a mineral.

With the availability of more extensive compositional data and more accurate values of standard free energies of formation, the phase diagrams could yield even better results. Also, the future availability of experimental data on quantitative ratios of various types of clay minerals in natural environments together with their corresponding water chemistry could help to correlate better with derived grades of mineral occurrences. Finally, the concept of fuzzy phase diagrams could be extended for modeling other complex mineralogical and geochemical systems.

ACKNOWLEDGMENTS

The author is grateful to Professor Kunal Ghosh, Professor M.K. Chakraborty and Dr D.K. Pal for their useful discussions and suggestions. This project was supported by the Department of Science & Technology, Government of India.

Supplementary Online Material (www.clays.org/journal/JournalDeposits.html)
Table S1
Program for construction of 2D fuzzy phase diagrams
Program for construction of 3D fuzzy phase diagrams

REFERENCES

Aja, S.U., Rosenberg, P.E. and Kittrick, J.A. (1991) Illite equilibria in solutions: I. Phase relationships in the system K_2O-Al_2O_3-SiO_2-H_2O between 25 and 250ºC. *Geochimica et Cosmochimica Acta*, **55**, 1353–1364.

Garrels, R.M. and Christ, C.L. (1965) *Solutions, Minerals and Equilibria*. Harper & Row, New York.

Helgeson, H.C., Brown, T.H. and Leeper, R.H. (1969) *Handbook of Theoretical Activity Diagrams Depicting Chemical Equilibria in Geologic Systems Involving an Aqueous Phase at One Atm and 0º to 300ºC* . Freeman, Cooper & Company, San Francisco.

Johnson, J.W., Oelkers, E.H. and Helgeson, H.C. (1992) SUPCRT92: A software package for calculating the standard molal thermodynamic properties of minerals, gases, aqueous species, and reactions from 1 to 5000 bars and 0 to 1000ºC. *Computers and Geosciences*, **18**, 899–947.

Klir, G. and Yuan, B. (1997) *Fuzzy Sets and Fuzzy Logic*, Prentice-Hall, New Delhi.

Kudrat, M., Sharma, K.P., Varadachari, C. and Ghosh, K. (1999) An algorithm and program in C-language for computation of standard free energy of formation of clay minerals. *Computers and Geosciences*, **25**, 241–250.

Kudrat, M., Varadachari, C. and Ghosh, K. (2000) Application of the improved regression method to derive ΔG_f^0 of non-stoichiometric clay minerals and their correlations with compositional parameters. *Chemical Geology*, **168**, 225–238.

Norton, D. (1974) Chemical mass transfer in the Rio Tanama system, west-central Puerto Rico. *Geochimica et Cosmochimica Acta*, **38**, 267–277.

Robie, R.A., Hemingway, B.S. and Fisher, J.R. (1978) Thermodynamic properties of minerals and related substances at 298.15ºK and 1 bar (10^5 pascals) pressure and at higher temperature. *US Geological Survey Bulletin*, **1452**, 1–456.

Tardy, Y. (1971) Characterisation of the principal weathering types by the geochemistry of waters from some European and African crystalline massifs. *Chemical Geology*, **7**, 253–271.

Tardy, Y. and Duplay, J. (1994) Stability fields of smectites and illites including glauconites as a function of temperature and chemical composition. Pp. 95–132 in: *Diagenesis IV* (K.H. Wolf and G.V. Chilingarian, editors). Developments in Sedimentology, **51**. Elsevier, Amsterdam.

Varadachari, C. (1992) Constructing phase diagrams for silicate minerals in equilibrium with an aqueous phase: A theoretical approach. *Soil Science*, **153**, 5–12.

Varadachari, C. and Ghosh, K. (2003) Thermodynamic derivation of new low temperature phase diagrams for phyllosilicates defining stable and metastable phases. *Indian Journal of Geology*, **75**, 203–217.

Varadachari, C. and Mukherjee, G. (2004) Discriminant analysis of clay mineral compositions. *Clays and Clay Minerals*, **52**, 311–320.

Varadachari, C., Kudrat, M. and Ghosh, K. (1994) Evaluation of standard free energies of formation of clay minerals by an improved regression method. *Clays and Clay Minerals*, **42**, 298–307.

Varadachari, C., Mukherjee, G., Goswami, D.P. and Chakraborty, M.K. (2003) Understanding clay minerals with fuzzy mathematics. *Naturwissenschaften*, **90**, 44–48.

(*Received 9 May 2005; revised 24 March 2006; Ms. 1043; A.E. Peter J. Heaney*)

APPENDIX

The methodology for deriving grades at a single point on the $\log[Si(OH)_4] - \log[K^+/H^+]$ space is illustrated here with only a small number of clay minerals. The dataset is assumed to consist of four species of clay minerals, *i.e.* two montmorillonites, three illites, two beidellites and one vermiculite (selected from Supplementary information Table S1). Inputs required are: (1) structural formulae of the minerals from composition data (without any residual charge), as shown in the second column of Table A1; (2) standard free energies of formation, ΔG_f^0, as shown in the third column, (3) standard free energy change of crystallization, ΔG_c^0 for a mineral of composition $K_\kappa Na_\nu Ca_\chi Si_\sigma Al_\alpha Mg_\lambda Fe(III)_\phi Fe(II)_\tau O_{10}(OH)_2$, obtained as the standard free energy change of the reaction: $\lambda Mg^{2+} + \kappa K^+ + \chi Ca^{2+} + \nu Na^+ + \phi FeO(OH) + \tau FeO + \alpha Al(OH)_3 + \sigma Si(OH)_4 \rightleftharpoons K_\kappa Na_\nu Ca_\chi Si_\sigma Al_\alpha Mg_\lambda Fe(III)_\phi Fe(II)_\tau O_{10}(OH)_2 + (2\lambda + \kappa + 2\chi + \nu)H^+ + [\{(\phi + 3\alpha + 4\sigma) - (2\lambda + \kappa + 2\chi + \nu + 2)\} \div 2].H_2O$. Values of ΔG_c^0 are shown in the fourth column. The free energy change for a given activity of ions in solution is evaluated as $\Delta G_c = \Delta G_c^0 - RT\ln[Si(OH)_4] - \kappa RT\ln[K^+/H^+] - \lambda RT\ln[Mg^{2+}/(H^+)^2] - \nu RT\ln[Na^+/H^+] - \chi RT\ln[Ca^{2+}/(H^+)^2]$, where symbols within parenthesis refer to activities in moles/L. For a phase diagram constructed in $\log[Si(OH)_4] - \log[K^+/H^+]$ axis, the values of the other parameters, *i.e.* $\log[Mg^{2+}/(H^+)^2]$, $\log[Na^+/H^+]$ and $\log[Ca^{2+}/(H^+)^2]$ are assigned constant values and ΔG_c is then evaluated over a range of values of $\log[Si(OH)_4]$ and $\log[K^+/H^+]$. In this example, ΔG_c has been evaluated for $\log[Mg^{2+}/(H^+)^2] = 10$, $\log[Na^+/H^+] = 6$, $\log[Ca^{2+}/(H^+)^2] = 14$ and for a single point on the $\log[Si(OH)_4] - \log[K^+/H^+]$ axis corresponding to $\log[Si(OH)_4] = -3$ and $\log[K^+/H^+] = 5$. Derived ΔG_c values are listed in column 5. The ΔG_c values for every mineral of a group are compared with the ΔG_c values of all other minerals of all other groups (column 6). The mineral with the more negative value of ΔG_c is selected and listed with a weightage of 1. Total weightage for each mineral type is obtained (column 7) and divided by the total weightage for all minerals. This gives the zonal grade for each type of mineral (last column) at a particular value of $\log[Si(OH)_4]$ and $\log[K^+/H^+]$.

Table A1. An example for obtaining fuzzy grades at $\log[Si(OH)_4] = -3$ and $\log[K^+/H^+] = 5$ at standard temperature and pressure with $\log[Mg^{2+}/(H^+)^2] = 10$, $\log[Na^+/H^+] = 6$, $\log[Ca^{2+}/(H^+)^2] = 14$.

Mineral	Composition	ΔG_f^0	ΔG_c^0	ΔG_c	Comparisons of ΔG_c → Result	Total weight	Grades
Illite 1 i(1)	$K_{0.5}Na_{0.08}Si_{3.46}$ $Al_{2.07}Mg_{0.27}$ $Fe^{III}_{0.23}$ $Fe^{II}_{0.07}O_{10}(OH)_2$	−1275.62	−9.776	−3.3637	i(1) > m(1) → m(1) i(1) < m(23) → i(1) i(1) > b(1) → b(1) i(1) < v(1) → i(1)		
Illite 22 i(22)	$K_{0.62}Na_{0.07}Si_{3.41}$ $Al_{2.34}Mg_{0.19}$ $Fe^{III}_{0.09}O_{10}(OH)_2$	−1298.4	−10.154	−3.5921	i(22) > m(1) → m(1) i(22) < m(23) → i(22) i(22) > b(1) → b(1) i(22) < v(1) → i(22)	Illite = 5	
Illite 24 i(24)	$K_{0.84}Na_{0.03}Si_{3.47}$ $Al_{2.2}Mg_{0.24}Fe^{III}_{0.05}$ $Fe^{II}_{0.01}O_{10}(OH)_2$	−1302.3	−6.0678	−1.1154	i(24) > m(1) → m(1) i(24) > m(23) → m(23) i(24) > b(1) → b(1) i(24) < v(1) → i(24)	Montmorillonite = 7 Beidellite = 5 Vermiculite = 0	Illite = 5/17 = 0.29 Montmorillonite = 7/17 = 0.41 Beidellite = 5/17 = 0.29
Mont 1 m(1)	$K_{0.22}Na_{0.72}Ca_{0.05}$ $Si_{3.9}Al_{1.671}Mg_{0.234}Fe^{III}_{0.14}$ $Fe^{II}_{0.0525}O_{10}(OH)_2$	−1264.83	−20.4179	−15.9976	m(1) < b(1) → m(1) m(1) < v(1) → m(1)	Total =17	Vermiculite = 0/17 = 0
Mont 23 m(23)	$K_{0.15}Ca_{0.12}Si_{3.69}$ $Al_{1.71}Mg_{0.26}$ $Fe^{III}_{0.4}O_{10}(OH)_2$	−1245.03	−11.1121	−2.8717	m(23) > b(1) → b(1) m(23) < v(1) → m(23)		
Beid 1 b(1)	$K_{0.19}Na_{0.03}$ $Si_{3.63}Al_{2.24}Mg_{0.07}$ $Fe^{III}_{0.01}O_{10}(OH)_2$	−1283.91	−25.2782	−13.8727	b(1) < v(1) → b(1)		
Verm 1 v(1)	$Si_{2.895}Al_{1.212}Mg_{3.2945}$ $Fe^{III}_{0.065}O_{10}(OH)_2$	−1357.63	57.343	24.363			